Rock Mechanics
and Rock Engineering 21, 119—137 (1988)

**Rock Mechanics
and Rock Engineering**

Design Charts for a Deep Circular Tunnel Under Non-uniform Loading

By

Emmanuel Detournay[1] and **Christopher M. St. John**[2]

[1] Dowell Schlumberger,Tulsa, OK, U. S. A.
[2] Principia Mechanica Ltd., London, U. K.*

Summary

This paper describes "design charts" which can be used to quickly predict the size and shape of the failed rock regions caused by the excavation of a deep tunnel, and the induced closure for cases of non-uniform *in-situ* stress fields. Through a simple graphical construction, the design charts can also be used to evaluate the performance of a support system.

Introduction

The redistribution of stress that accompanies the excavation of a deep tunnel may induce failure of the rock. Under such circumstances, the role of the support system may be understood as controlling the extent of the failed region around the tunnel, and, hence, limiting closure of the tunnel walls to an acceptable amount. The selection of a support system required to meet such performance criteria is generally based on application of the concept of the ground reaction curve (GRC). The latter can be briefly described as the relationship between the pressure exerted by a support system and the corresponding excavation induced displacement of the tunnel wall.

To calculate a GRC, it is postulated that support forces equivalent to the pre-excavation stresses are applied at the instant of excavation, thereby inhibiting any deformation of the rock. The support forces are then relaxed, and the corresponding induced displacement of the tunnel is calculated. Because of the analytical simplicity, calculation of the GRC has been performed widely for the case of a circular tunnel under a uniform initial stress field. In those calculations, the rock is generally treated as an elastoplastic material characterized by a cohesive-frictional yield strength and by dilatation during plastic deformation. Brown et al. (1983) provide an exhaustive list of references of such simple analytical models, and discuss different characterizations of the annulus of failed rock around the tunnel.

* Previously of J. F. T. Agapito and Associates, U. S. A.

A recent analytical development (Detournay, 1985, 1986a) has facilitated the generalization of the GRC concept for some cases of non-uniform *in-situ* stress fields (Detournay and Fairhurst, 1982). As an application of that development, this paper describes design charts that provide a powerful means of performing parametric analyses of tunnels subject to non-uniform loading. The design charts consist of contour maps of the induced tunnel wall displacement in the direction of the principal *in-situ* stresses. These contour maps, which are calculated for the case of an unsupported tunnel, allow a user to quickly predict the minimum and maximum closure experienced by the tunnel during excavation unloading of the rock mass. Also, a simple geometrical construction can be used to assess the influence of ground support on tunnel closure.

This paper starts with a brief discussion that is intended to establish the utility of the design charts. The theoretical basis for the charts and the calculations upon which they rely are then described in sufficient detail for a user to understand the scope and limitations of their application. Finally, a practical example of the use of one of the charts is provided, with particular attention paid to the method of evaluating the influence of internal pressure provided by a ground support system. An appendix contains a series of charts that cover the range of properties likely to be encountered in many practical circumstances.

The Design Chart

The mode of behavior of the rock mass around a circular tunnel can be depicted graphically in a normalized stress diagram with axes P_o/q and S_o/q, (P_o and S_o denote, respectively, the *in-situ* mean stress and stress deviator in a plane perpendicular to the tunnel axis, and q designates the uniaxial compressive strength of the rock). Such a graphical construction is illustrated by Fig. 1, in which the following four regions are identified:

- Region I, within which the rock mass behaves as a linear elastic material, since the state of stress does not exceed the strength at any point;
- Region IIa, within which failure of the rock around the tunnel will extend in a direction perpendicular to the more compressive principal applied stress, but not completely engulf the tunnel;
- Region IIb, within which the tunnel will be completely surrounded by an oval-shaped failure zone; and,
- Region III, within which a butterfly-shaped failure zone may develop.

The above rules provide a very simple means of immediately identifying the general behavior of the rock mass around a tunnel. (Note that figures similar to Fig. 1 must be prepared for a specific friction angle.) If the stress state plots within Regions I and II, then the methods described in this paper can be used to calculate the displacements of the tunnel wall due

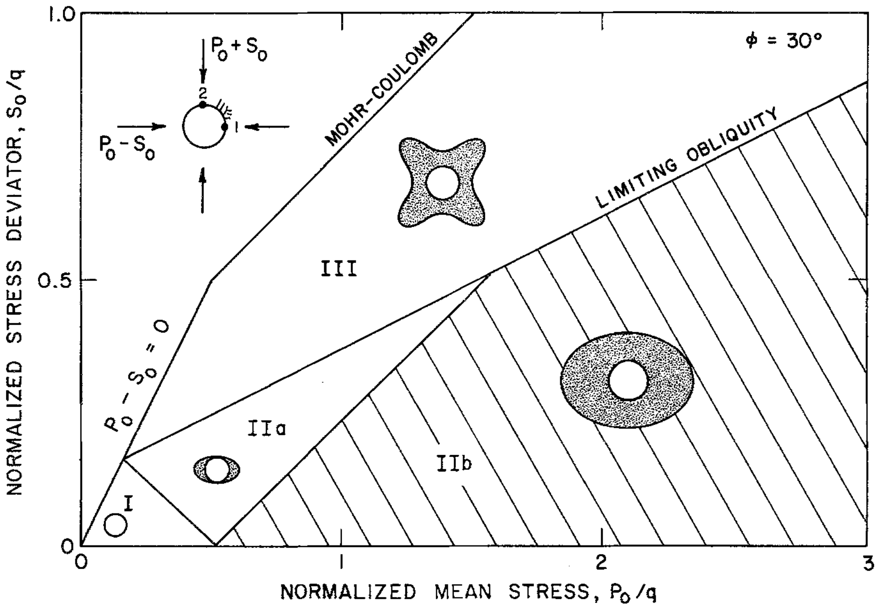

Fig. 1. Relationship between the initial stress state and failure modes for an unsupported circular

to excavation. On the other hand, if the stress state lies in Region III, then a numerical modeling technique, such as one based on the finite difference or finite element methods, will have to be used to investigate the deformation of the rock mass around the tunnel. Note that Region III is bounded by three lines: one is the boundary between II and III (its definition is deferred to a later section); the second, labelled $P_o - S_o = 0$, corresponds to a uniaxial *in-situ* stress field; the third delimits the *in-situ* stress according to the Mohr-Coulomb limit equilibrium line (i.e., it is assumed that the *in-situ* stress corresponds to an elastic state for the rock).

It has been stated above that the behavior of an unsupported tunnel can be related, for a specific value of the rock friction angle, to the normalized values P_o/q and S_o/q of the mean and deviatoric stresses. Closure of the tunnel during plastic deformation is related to those same quantities. It will subsequently be shown that actual closure can be naturally normalized by the quantity $aq/2G$, in which a is the tunnel radius and G the shear modulus of the rock; and that the normalized closure for an unsupported tunnel depends only on P_o/q and S_o/q, provided that the friction angle, ϕ, the dilatation angle, ϕ^*, and Poisson's ratio, ν of the rock are fixed. The normalized radial displacement at the tunnel wall along diameters perpendicular and parallel to the major *in-situ* stress $P_o + S_o$ can thus be displayed in the form of contour lines in the stress diagram (P_o/q, S_o/q). (See Fig. 2, where, by convention, the solid line refers to the radial displacement perpendicular to the major *in-situ* stress direction, the dashed line to the displacement parallel to that direction).

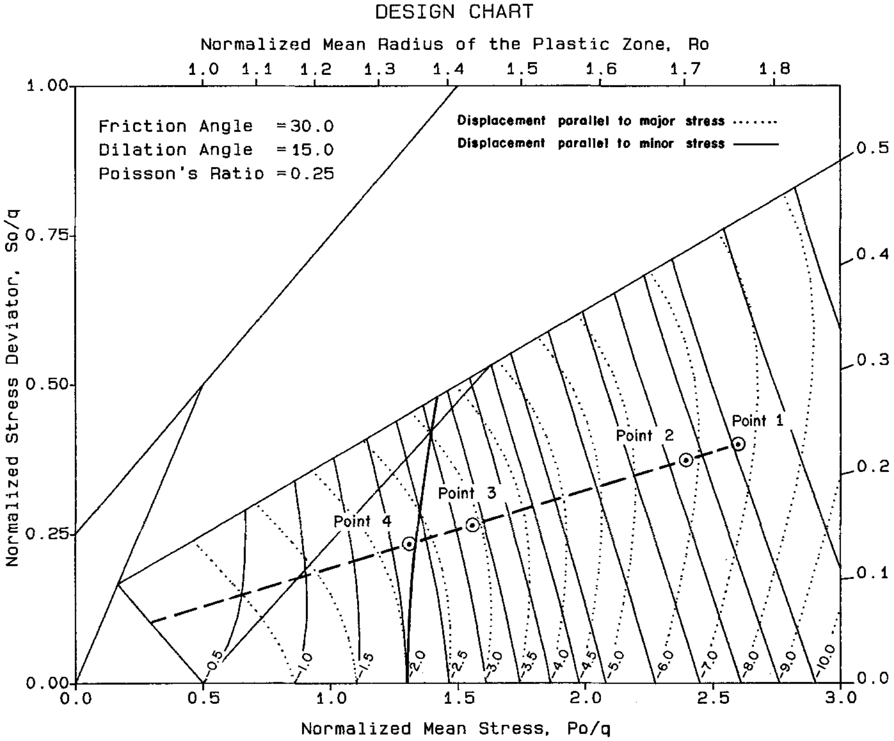

Fig. 2. Design chart for a material characterized by friction angle of 30°, dilatation angle of 15°, and Poisson's ratio of 0.25

The user of the design charts first selects a chart for the appropriate set of rock properties (ϕ, ϕ^*, ν). From the initial state of stress and the uniaxial compressive strength of the rock mass the normalized mean and deviatoric stresses are calculated, and the corresponding point is plotted on the design chart. If the point lies anywhere within zone II, then the normalized radial displacement of the wall of the tunnel (measured at points on the diameters of the tunnel parallel to the major and minor *in-situ* stresses) can be interpolated from the displacement contours. The displacement can then be transformed to the physical values by multiplying by the factor $aq/2G$. An example serves to illustrate this process.

Consider the following set of conditions:

in-situ vertical stress		30 MPa
in-situ horizontal stress		22 MPa
Tunnel radius		2.5 m
Rock Mass Shear Modulus	(G)	800 MPa
Poisson's ratio	(ν)	0.25
Uniaxial Strength	(q)	10 MPa
Friction Angle	(ϕ)	30°
Dilatation Angle	(ϕ^*)	15°

From these data the normalized mean and deviator stresses are 2.6 and 0.4, respectively. Those values define Point 1 on Fig. 2. Hence behavior type IIb is expected, and the normalized values of the displacement are 10.3, from the solid contours and 6.7 from the dashed contours. The normalization factor on the closures is 1.56 cm, so the calculated displacements are approximately 16.1 cm and 10.5 cm. The larger value was associated with the solid contours and is, therefore, the displacement perpendicular to the direction of the major *in-situ* stress. Additional information about the extent and shape of failure and the influence of any ground support can also be obtained from the design chart. However, discussion of those refinements is deferred until after presentation of the relevant theoretical basis.

The Elastoplastic Model of a Deep Tunnel

Consider a long cylindrical tunnel of radius a in an infinite rock mass subject to a non-uniform *in-situ* stress. It is assumed that the long axis of the cavity is parallel to one of the principal *in-situ* stress directions and that the tunnel is deep enough so that the gravity force can be neglected. The rock is assumed to behave as an elastic perfectly plastic Mohr-Coulomb material; i.e., it is characterized by a yield envelope

$$\sigma_1 - K_p \sigma_3 - q = 0, \tag{1}$$

where K_p is the passive coefficient defined as $K_p = (1+\sin\phi)/(1-\sin\phi)$ and σ_1 and σ_3 are the major and minor principal stresses in the plane perpendicular to the tunnel axis. (Compressive stresses are taken as positive throughout this paper). Further, it is assumed that dilatant behavior during plastic flow is controlled by the flow rule,

$$d\varepsilon_3^p = -K_p^* d\varepsilon_1^p, \tag{2}$$

where K_p^* is the dilatation factor, $K_p^* = (1+\sin\phi^*)/(1-\sin\phi^*)$, ϕ^* is the dilatation angle, with $0 < \phi^* < \phi$, and $d\varepsilon_1^p$ and $d\varepsilon_3^p$ are the principal components of the incremental plastic strain tensor.

The *in-situ* stresses can be expressed in terms of the mean and deviatoric components, previously identified as P_o and S_o. Since the rock obeys the Mohr-Coulomb yield criterion, the deviatoric invariant S_o must be less than the limiting value S_o^l given by,

$$S_o^l = \frac{K_p - 1}{K_p + 1}\left(P_o + \frac{q}{K_p - 1}\right), \tag{3}$$

which is the equation of the limiting equilibrium line depicted in Fig. 1. This constraint on the *in-situ* stress can similarly be expressed by imposing that the obliquity, m, of the *in-situ* stress, defined as

$$m = S_o / S_o^l, \tag{4}$$

be less than 1.

We are concerned with prediction of tunnel closure caused by excavation unloading of the rock mass. In two-dimensional models, excavation unloading is simulated by removing the traction forces that were acting across the tunnel boundary prior to excavation. This load history has to be precisely defined since the solution of elastoplastic problems is generally dependent on the load path. In the present case the load trajectory selected involves first an elastic stage during which the boundary of the tunnel is unloaded until there is a uniform internal pressure p_e, at which the elastic limit of the rock is reached. The internal pressure is then reduced until the tunnel boundary becomes stress-free. Note that this load history is feasible, only provided that $m<0.5$. Indeed, if $m<0.5$, it can easily be proven, on the basis of Kirsch's solution, that there exists an interval of internal pressure values for which the rock remains elastic.

For the sake of convenience, we designate by 1 and 2 the points on the tunnel wall which are located on diameters respectively perpendicular and parallel to the major principal *in-situ* stress (see Fig. 1). The limiting internal pressure, p_e, is given by

$$p_e = \frac{2\,S_o^l}{K_p-1}\left(1+2\,m\frac{K_p-1}{K_p+1}\right) - \frac{q}{K_p-1}. \tag{5}$$

If the internal pressure, p, is decreased below this elastic limit, two isolated plastic regions will develop on either side of the tunnel in the vicinity of points 1, i.e., in a direction perpendicular to the maximum compressive *in-situ* stress. These two zones will eventually coalesce to form a unique yield region around the tunnel.

Extent and Shape of the Plastic Region

The mathematical analysis for determining the shape and extent of the failed rock region is based on the *a-priori* hypotheses that during excavation unloading of the rock mass:

1. The rock, once it has yielded, does not return to an elastic state (i.e., no elastic unloading).
2. The position of the boundary between intact and failed rock is statically determined by the internal pressure p and the *in-situ* stress.

These two assumptions, which are met in the uniform loading case, imply that the progressive removal of the preexisting traction forces on the boundary of the tunnel is accompanied by a progressive growth of the failed rock region; and, that the shape and extent of that region depends on the yield parameters (the friction angle ϕ and the unconfined compressive strength q), but not on the elasticity parameters G and ν and the dilatation angle ϕ^*.

The two *a-priori* hypotheses further imply that the stress field in the plastic zone is completely determined by the shape of the tunnel boundary, and by the stress conditions on that boundary. The stress field in the yield zone is thus characterized by a radial symmetry. Its solution is well-known (e.g., Salencon, 1967; Newmark, 1970) and given by

$$\sigma_{rr} = \left(p + \frac{q}{K_p - 1}\right)\left[\frac{r}{a}\right]^{K_p - 1} - \frac{q}{K_p - 1},$$

$$\sigma_{\theta\theta} = K_p\left(p + \frac{q}{K_p - 1}\right)\left[\frac{r}{a}\right]^{K_p - 1} - \frac{q}{K_p - 1},$$

$$\sigma_{r\theta} = 0. \tag{6}$$

With the stress in the yield zone known, the position of the elastoplastic interface is controlled by the condition that all stress components must be continuous across it (Kachanov, 1970).

The problem of determining the position of the elastoplastic interface, once the tunnel is completely surrounded by failed rock, is related to the problem solved by Galin (1946) (see also Prager and Hodge, 1968, and Hill, 1967) for the case of an incompressible frictionless Tresca material. As in the original solution of Galin, determination of the interface can be reduced to the problem of finding a mapping function, by using the Muskhelishvili (1962) complex variable method for solving plane elastic boundary value problem (Detournay, 1985, 1986a). The elastoplastic interface is found to be an oval characterized by a mean radius $a\ R_o$, where

$$R_o = \left[\frac{2}{K_p + 1}\ \frac{P_o + \dfrac{q}{K_p - 1}}{p + \dfrac{q}{K_p - 1}}\right]^{1/(K_p - 1)}, \tag{7}$$

and by a major to minor axis ratio given by

$$\frac{\text{Major} - \text{axis}}{\text{Minor} - \text{axis}} = \left(\frac{1 + m}{1 - m}\right)^{2/(K_p + 1)}. \tag{8}$$

The major axis of the interface is always perpendicular to the major compressive stress $(P_o + S_o)$ at infinity, and the mean radius of the plastic zone corresponds to the radius of the circular interface that would be obtained by neglecting the deviatoric component of the *in-situ* stress. From Eq. (8) it is apparent that the shape of the interface is controlled by only two parameters; the obliquity m and the friction angle ϕ. Further, because the shape of the plastic region is independent of p, the interface grows in a self-similar manner as the pressure is monotonically reduced below a minimum pressure p_l

$$p_l = \frac{2\,S_o^l}{K_p - 1}\;\frac{(1-m)^{2(K_p-1)/(K_p+1)}}{1+\left[\dfrac{K_p-1}{K_p+1}\right]^2 m^2} - \frac{q}{K_p-1}, \tag{9}$$

that corresponds to the condition when the interface is tangent to the tunnel boundary. This self-similar growth implies that there is indeed no elastic unloading, which is consistent with the first a-priori hypothesis. The other assumption — that the problem is statically determined — is met, provided that the obliquity m is less than a critical value m^*, which is a function of the friction angle ϕ. Table 1 lists the critical obliquity m^* that was calculated by considering the condition for which one of the slip-lines becomes tangent to the interface (Detournay, 1986a). If the obliquity is greater than m^* (but less than 1), the location of the elastoplastic interface is statically indeterminate. In that case, the stress field in the plastic zone is no longer given by Eq. (6), thus requiring a much more complicated process of solution (because of the need to simultaneously solve for the incremental stress and displacement fields for a small variation of the boundary conditions along the loading path). As a consequence, the location of the elastoplastic interface for obliquity greater than m^* depends also on the deformation characteristics of the rock, as well as upon the state of stress. Specifically it will be influenced by the shear modulus G, the Poisson's ratio ν, and the dilatation angle ϕ^*.

Table 1. *Critical Obliquity* m^*

ϕ	0	10°	20°	30°	40°
m^*	0.414	0.437	0.466	0.500	0.542

Relationship Between *in-situ* Stress and Failure

From the previous analysis, it is possible to develop the picture of the relationship between the *in-situ* stress and modes of failure around the tunnel that was presented at the beginning of the paper. The relationship was depicted graphically in Fig. 1, which illustrated the nature of any failed rock region around an unsupported tunnel for various combinations of *in-situ* deviatoric and mean stresses. The figure identified the four different types of behavior discussed earlier, and it suffices here to note that Region II on the figure corresponds to statically determinate cases, and Region III to statically indeterminate ones. The boundary between II and III is the line of critical obliquity m^*. (This line, like any other line of constant obliquity passes through the intersection of the Mohr-Coulomb yield envelope with the mean stress axis.) As noted earlier, statically determinate cases can be solved semi-analytically (at least in Region IIb), while statically indeterminate conditions must presently be solved by means of numerical techniques. Within this paper, discussion is confined to the statically determinate cases that can be analyzed using the design charts.

Closure of the Tunnel

With the problem of evolution of the failed rock region resolved — at least for mode II — calculation of the tunnel closure during excavation unloading can be undertaken. This computation involves first determination of the elastic displacement at the failed-intact rock boundary, then integration of a system of two hyperbolic partial differential equations governing the displacement in the plastic region (Detournay and Fairhurst, 1987).

Calculation of the displacement at the elastic boundary can be carried out analytically, by simple application of Mushkelishvili's theory, but integration of the equations governing the displacement in the plastic zone must be performed numerically by the method of characteristics (Masseau, 1899). These governing equations are obtained on the basis of the following argument. Since the principal stress directions in the plastic zone are radial and tangential — due to the statically determinate nature of the problem — the principal directions of the incremental plastic strain tensor remain oriented along the radial and tangential directions. The flow rule (2) can thus be integrated to yield

$$\varepsilon_r^p + K_p^* \varepsilon_\theta^p = 0; \;\; \varepsilon_{r\theta}^p = 0. \tag{10}$$

The partial differential equations for the displacements are then derived from (10), using the decomposition of the strain into plastic and elastic parts and the strain-displacement relationship (the elastic strain can be found explicitly from Eq. (6) for the stress in the yield zone).

The lack of solution for the elastoplastic boundary in the early stage of rock failure (when the internal pressure p is in the range $p_l < p < p_e$) does not preclude calculation of tunnel closure for $p < p_l$. Closure of the tunnel in the early stage ($p_l < p < p_e$) can be assessed by interpolating quadratically from the closure computed at p_e and p_l, noting also that the rate of closure with p at the elastic limit can be calculated from Kirsch's solution.

If the evolution of tunnel closure as a function of the internal pressure is desired (Ground Reaction Curve), the methodology of calculation of the displacement does not need to be repeated for a series of values of the internal pressure. In other words, there is no need to solve a sequence of Cauchy problems for each new position of the elastoplastic interface. Indeed, the self-similar growth of the interface, for internal pressure less than p_e, implies that as in the uniform loading case (Detournay, 1986b), the differential equations for the displacement field can be solved in a unit-plane; which is defined by dividing all physical lengths by the characteristic size aR_o of the plastic zone. In the unit plane, the interface occupies a fixed position which separates an interior plastic region from an exterior elastic one; the image of a physical point in the unit plane moves along a radial line, towards the origin, as the interface is growing. As a consequence, the general expression for the displacement field in the plastic zone is

$$\underline{u} = \frac{a S_o^l}{2G} R_o \tilde{\underline{u}} (\rho, \theta; m, \phi, \phi^*, \nu). \tag{11}$$

The field $\tilde{\underline{u}}$ is only a function of the coordinates (ρ, θ) of the unit plane $(\rho = r/a R_o)$, and depends on four parameters m, ϕ, ϕ^* and ν. Once $\tilde{\underline{u}}$ has been calculated, the physical displacement at any point, and at any stage of the loading, can be retrieved by a simple scaling operation. In particular, if only closure in the vertical and horizontal directions is of interest, then $\tilde{\underline{u}}$ needs to be calculated along the x and y axes in the unit plane; and the boundary displacement at points 1 and 2 as a function R_o is then given by (11), taking $\rho = 1/R_o$ and with $\theta = 0°$ or $90°$. We can thus formally write the displacement, U_1 and U_2, at points 1 and 2 respectively, as

$$U_i = \frac{a q}{2G} U_i^*, i = 1, 2 \tag{12}$$

where the normalized displacement U_i^* is a function of the form

$$U_i^* = \frac{S_o^l}{q} F_i(R_o, m; \phi, \phi^*, \nu). \tag{13}$$

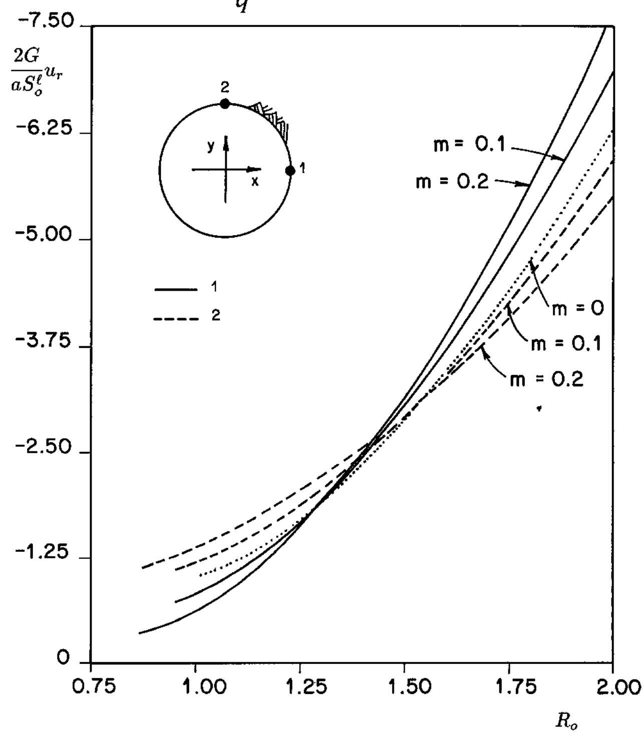

Fig. 3. Normalized Radial Displacement as a Function of the Mean Radius of the Plastic Zone. ($K_p = 3$, $K_p^* = 1.42$, $\nu = 0.25$)

Note, however, that since the method of characteristics is a discrete method, the function $\tilde{\underline{u}}$ can only be calculated at some discrete points of the unit-plane, and therefore closure can only be computed for discrete values of the internal pressure.

Figure 3 depicts the variation of the tunnel wall displacement (normalized here by $a S_o^l/2\,G$) as a function of the characteristic size R_o of the failed rock region for an *in-situ* stress characterized by $m = 0$ (uniform loading), $m = 0.1$ and $m = 0.2$. This figure illustrates that with the existence of a deviatoric component ($S_o > 0$) in the initial stress field, the circular tunnel becomes oval during closure accompanying excavation-unloading of the rock mass. The directions of minimum and maximum closure will always be parallel to the principal directions of the *in-situ* stress field; however, the direction of maximum closure may be either parallel or perpendicular to the major principal stress. In the early stage of failure, the induced radial displacement is maximum at Points 2; but if rock failure propagates deep enough into the rock mass, closure becomes greater along the diameter passing through Points 1.

The average displacement corresponds to the displacement U_o^* calculated for uniform loading P_o. This displacement is given by (e.g., Newmark, 1970; Detournay, 1986b)

$$\frac{q}{S_o^l}\,U_o^* = 1 + \frac{\lambda + 2\,K_p + 2\,K_p^*}{(K_p^* + 1)\,(K_p^* + K_p)}\,(R_o^{1+K_p^*} - 1) + \frac{\lambda}{(K_p - 1)\,(K_p^* + K_p)}\,(R_o^{1-K_p} - 1), \tag{14}$$

where

$$\lambda = (K_p - 1)\,(K_p^* - 1) + (1 - 2\,\nu)\,(K_p + 1)\,(K_p^* + 1). \tag{15}$$

(Displacement U_o^* is taken positive towards the center of the tunnel).

Let us examine now the construction of the design charts. Taking into account Eq. (7) with $p = 0$ and Eq. (4), the general expression (12) for the induced boundary displacement U_i can be rewritten as

$$U_i = \frac{a\,q}{2\,G}\,U_i^*\left(\frac{P_o}{q}, \frac{S_o}{q}; \phi, \phi^*, \nu\right), \quad i = 1, 2. \tag{16}$$

Thus by imposing the friction angle ϕ, the dilatation angle ϕ^* and the Poisson's ratio ν, the normalized displacement U_i^* and U_2^* can be contoured in the stress space defined in Fig. 1. A typical example was illustrated in Fig. 2 (note that both contours are labeled at their common root, which corresponds to a uniform *in-situ* stress state).

The locus of the non-uniform *in-situ* stress sates, that would result in uniform closure of the tunnel, is also displayed in the normalized stress diagram (P_o/q, S_o/q). This locus is determined by the intersection of two contour lines that originate from the same point on the P_o/q axis. To left of that locus, closure is greater in the direction of the maximum *in-situ* stress; to the right, closure is greater in the direction of the minimum *in-situ* stress.

Support Pressure

The effect of a uniform support pressure p can be taken into account by means of a simple geometrical construction. According to Eq. (13), closure of the tunnel is fundamentally controlled by the position of the elastoplastic interface. It thus follows from Eqs. (4) and (7) that closure of a tunnel subject to an internal pressure p in a far-field stress characterized by a mean stress P_o and a deviatoric stress S_o is proportional to the closure of an unsupported tunnel in an *in-situ* stress field of the same obliquity, but characterized by a mean stress $P'_o = P_o - \Delta P_o$ with

$$\Delta P_o = \frac{p(K_p - 1)}{q + p(K_p - 1)} \left(P_o + \frac{q}{K_p - 1} \right), \tag{17}$$

in which the factor of proportionality is given by S^l_o / S'^l_o, and S'^l_o is the limiting *in-situ* stress deviatoric corresponding to P'_o. The effect of an internal pressure can thus be accounted for by shifting the initial stress point $(P_o/q, S_o/q)$ along a line of constant obliquity (the support pressure line), by an amount $-\Delta P_o/q$, measured along the horizontal axis; and multiplying the measured displacement by the factor S^l_o / S'^l_o. This procedure is applicable provided that the new stress point $(P'_o/q, S'_o/q)$ remains within Region II. The internal pressure, which moves the stress point $(P'_o/q, S'_o/q)$ to the boundary between Regions I and II, represents the support pressure required to prevent any yielding of the rock and can, therefore, also be derived from Eq. (5).

Two other items of information have been displayed on the design charts, of which Fig. 2 is a typical example. First, the normalized mean radius, R_o, of the plastic zone is marked along the upper margin of the frame; second, the obliquity of the *in-situ* stress is indicated along the right-hand edge of the figure. The latter can be used in conjunction with Eq. (8) to calculate the eccentricity of the failed region.

The earlier example of the application of the design charts considered the case of an unsupported tunnel. Displacements of 16.1 cm and 10.5 cm at the springline and at the crown were calculated from the normalized closures interpolated from Fig. 2. The effect of ground support can be assessed by first constructing the constant obliquity line through point 1, which was defined by the normalized *in-situ* stresses P_o/q and S_o/q. The correction to the normalized mean stress for a support pressure p and the parameters of this problem are from Eq. (17):

$$\frac{\Delta P_o}{q} = \frac{3.1\, p/q}{0.5 + p/q}. \tag{18}$$

Hence, for a case of heavy rockbolting, providing an internal support pressure of 0.34 MPa (Hoek and Brown, 1980), the corrected normalized mean stress is 2.4. This value and the "support pressure line" define point 2 at which the springline and crown displacements are respectively 13.3 cm and 9.0 cm, for an unsupported tunnel. Correcting these values by the factor $S_o^l/S_o'^l$, here equal to (3.8/3.7), the springline and crown displacements are thus equal to 13.7 cm and 9.2 cm. Points 3 and 4 correspond to much higher support pressures, such as might be provided by closely spaced steel sets ($p = 2.4$ MPa) and a 30 cm concrete liner ($p = 3.4$ MPa). Note that the tunnel closure is nearly uniform for the case of the thick concrete liner, even though an oval plastic region has developed.

Conclusion

The design charts described in this paper constitute a powerful engineering tool for estimating the support requirement and the closure of a deep cylindrical tunnel for cases for which the problem is statically determinate. Besides providing a rapid means to calculate the support pressure required to limit closure to some specified amount, the design charts also display information on the extent and shape of the plastic zone. The latter information is particularly important in the design of rockbolted tunnel sections. The use of dimensionless quantities enables the design charts to be generated for only three independent material parameters, ϕ, ϕ^*, and ν. The design charts can be prepared easily and rapidly on a micro-computer equipped with a pen-plotter.

Appendix: Selected Design Charts

This appendix comprises nine design charts prepared for a range of material properties. As noted in the paper, the data on the charts is presented in normalized form, but must be prepared for specific values of the friction angle, dilatation angle, and Poisson's ratio. Since the displacements are least influenced by Poisson's ratio, emphasis has been placed on providing charts for a range of friction and dilatation angles. A single value of Poisson's ratio for each friction angle was selected on the basis that

$$1 - 2\,\nu \leq \sin\phi,$$

for the out-of-plane stress to remain intermediate (Detournay, 1986a).

The charts presented in this Appendix were prepared using a FORTRAN program which can be executed on an IBM-PC or compatible microcomputer. The program writes data files that directly drive a Hewlett Packard 7475A (or similar) pen plotter.

Acknowledgement

The work described in this paper is based on the results of investigations supported by the National Science Foundation and the Defense Nuclear Agency.

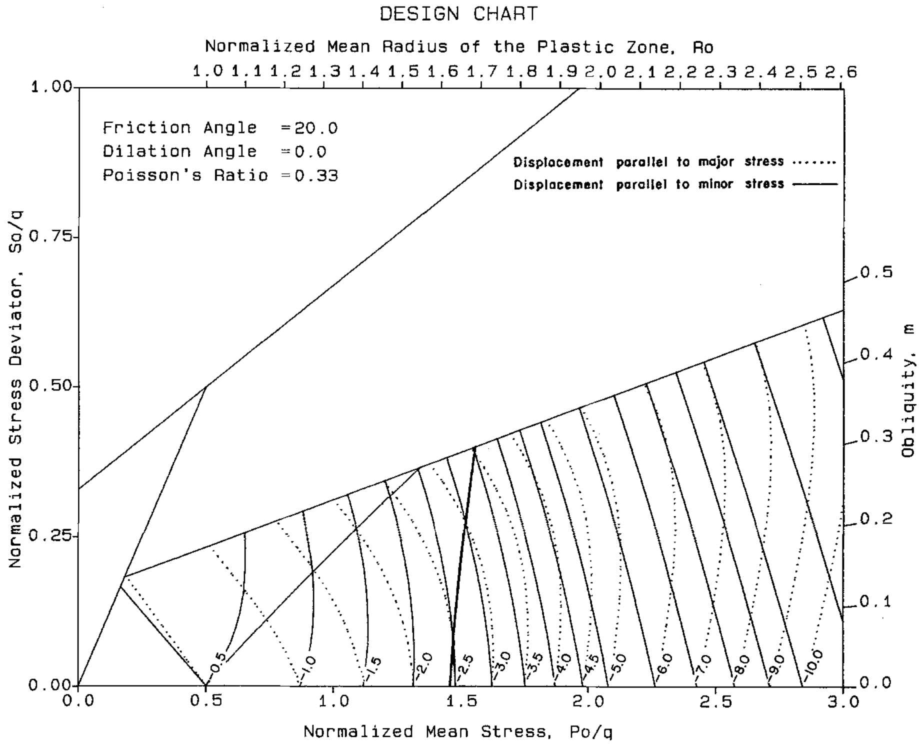
DESIGN CHART
Normalized Mean Radius of the Plastic Zone, Ro
1.0 1.1 1.2 1.3 1.4 1.5 1.6 1.7 1.8 1.9 2.0 2.1 2.2 2.3 2.4 2.5 2.6
Friction Angle =20.0
Dilation Angle =0.0
Poisson's Ratio =0.33
Displacement parallel to major stress
Displacement parallel to minor stress
Normalized Stress Deviator, So/q
Obliquity, m
Normalized Mean Stress, Po/q

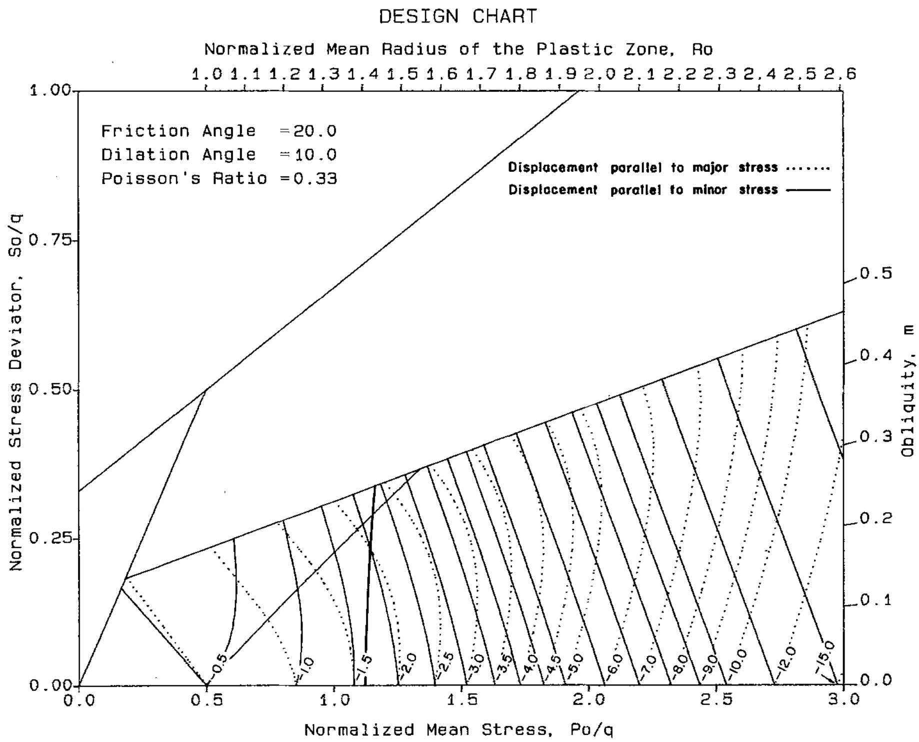
DESIGN CHART
Normalized Mean Radius of the Plastic Zone, Ro
1.0 1.1 1.2 1.3 1.4 1.5 1.6 1.7 1.8 1.9 2.0 2.1 2.2 2.3 2.4 2.5 2.6
Friction Angle =20.0
Dilation Angle =10.0
Poisson's Ratio =0.33
Displacement parallel to major stress
Displacement parallel to minor stress
Normalized Stress Deviator, So/q
Obliquity, m
Normalized Mean Stress, Po/q

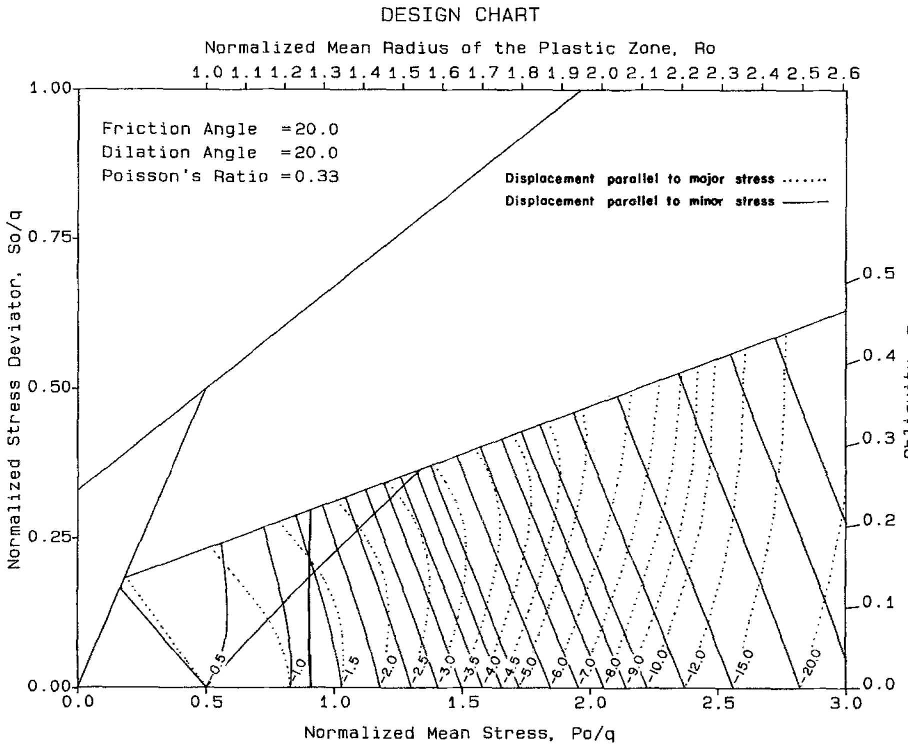
DESIGN CHART
Normalized Mean Radius of the Plastic Zone, Ro
1.0 1.1 1.2 1.3 1.4 1.5 1.6 1.7 1.8 1.9 2.0 2.1 2.2 2.3 2.4 2.5 2.6
Friction Angle =20.0
Dilation Angle =20.0
Poisson's Ratio =0.33
Displacement parallel to major stress ....
Displacement parallel to minor stress ———
Normalized Stress Deviator, So/q
Obliquity, m
Normalized Mean Stress, Po/q
0.5
1.0
1.5
2.0
2.5
3.0
3.5
4.0
4.5
5.0
6.0
7.0
8.0
9.0
10.0
12.0
15.0
20.0

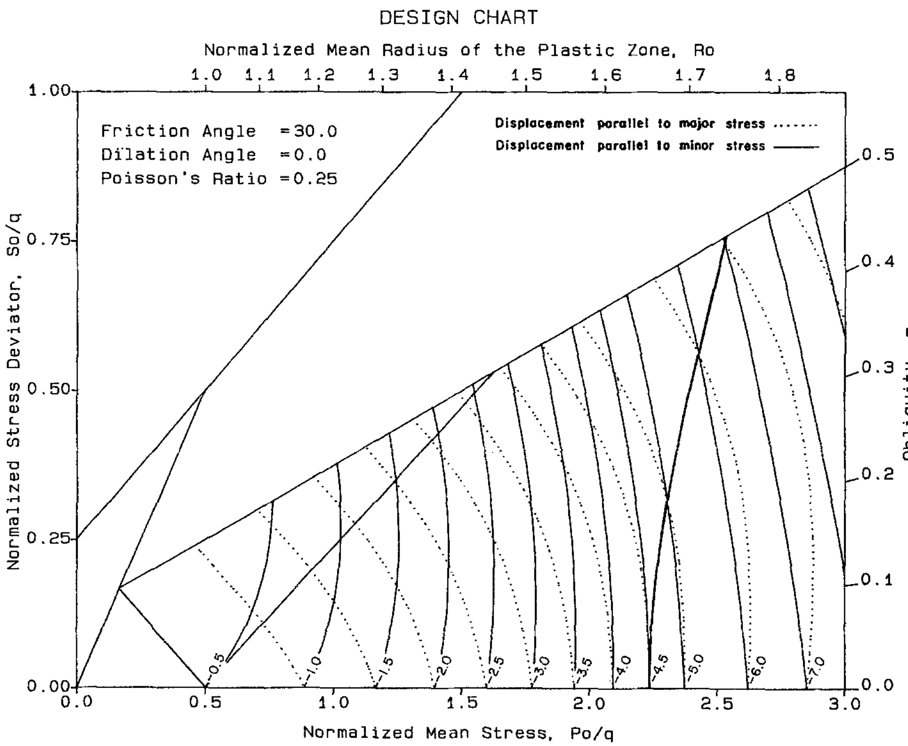
DESIGN CHART
Normalized Mean Radius of the Plastic Zone, Ro
1.0 1.1 1.2 1.3 1.4 1.5 1.6 1.7 1.8
Friction Angle =30.0
Dilation Angle =0.0
Poisson's Ratio =0.25
Displacement parallel to major stress ....
Displacement parallel to minor stress ———
Normalized Stress Deviator, So/q
Obliquity, m
Normalized Mean Stress, Po/q
0.5
1.0
1.5
2.0
2.5
3.0
3.5
4.0
4.5
5.0
6.0
7.0

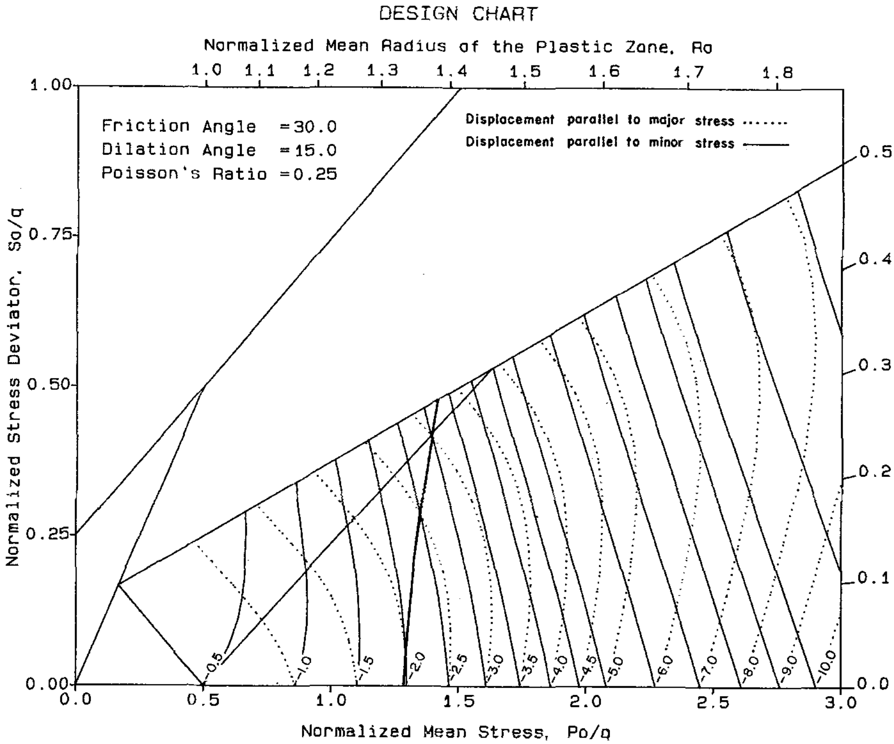
DESIGN CHART
Normalized Mean Radius of the Plastic Zone, Ro
Friction Angle =30.0
Dilation Angle =15.0
Poisson's Ratio =0.25
Displacement parallel to major stress
Displacement parallel to minor stress
Normalized Stress Deviator, So/q
Obliquity, m
Normalized Mean Stress, Po/q

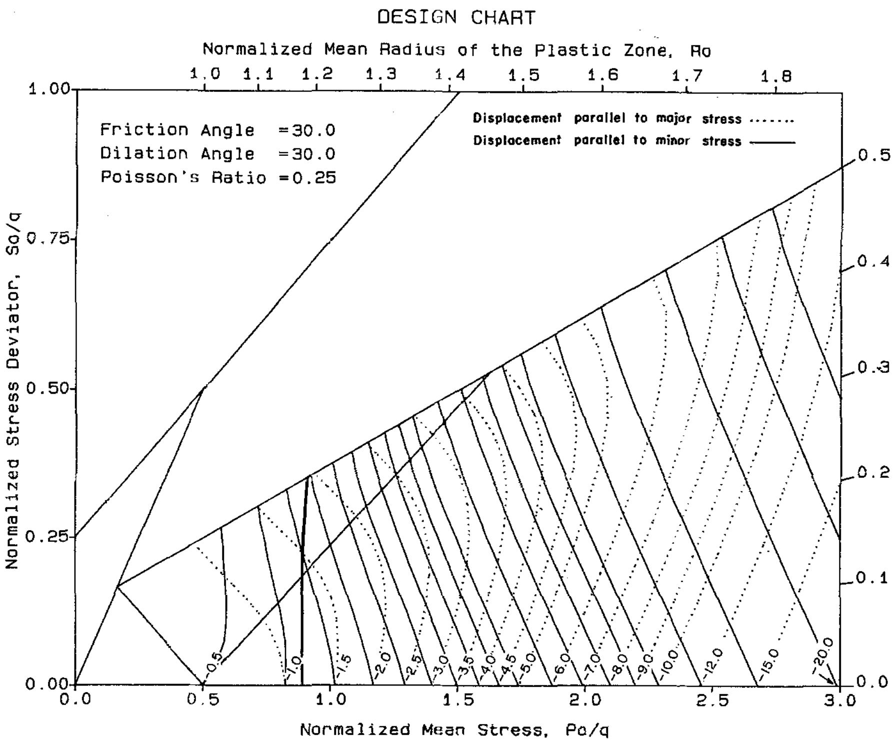
DESIGN CHART
Normalized Mean Radius of the Plastic Zone, Ro
Friction Angle =30.0
Dilation Angle =30.0
Poisson's Ratio =0.25
Displacement parallel to major stress
Displacement parallel to minor stress
Normalized Stress Deviator, So/q
Obliquity, m
Normalized Mean Stress, Po/q

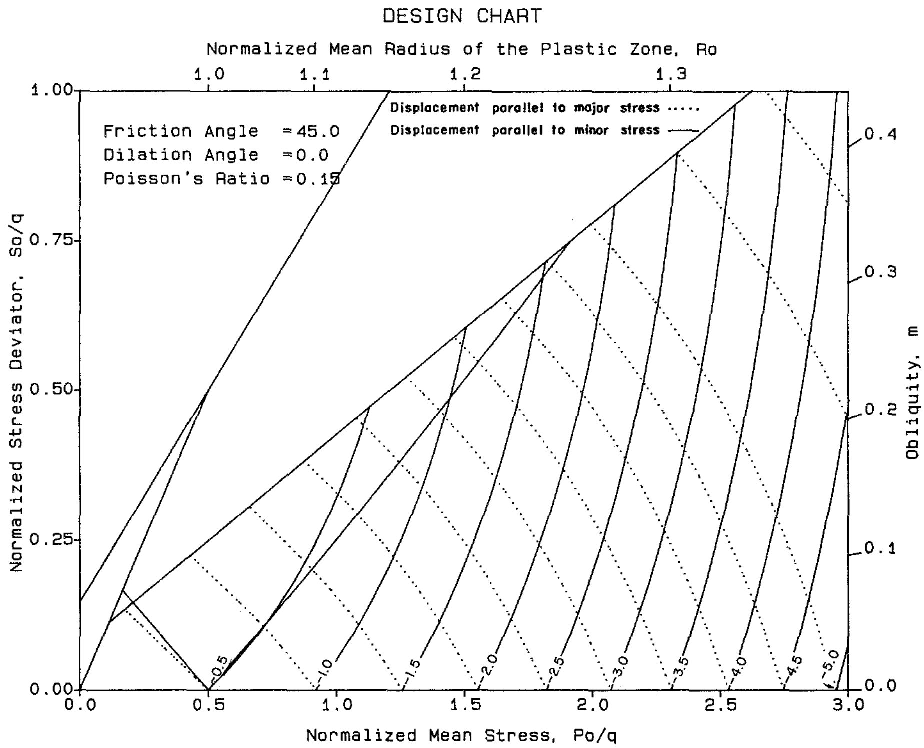
DESIGN CHART
Normalized Mean Radius of the Plastic Zone, Ro
1.0
1.1
1.2
1.3
Displacement parallel to major stress .....
Displacement parallel to minor stress ——
Friction Angle =45.0
Dilation Angle =0.0
Poisson's Ratio =0.15
Normalized Stress Deviator, So/q
1.00
0.75
0.50
0.25
0.00
Obliquity, m
0.4
0.3
0.2
0.1
0.0
0.5
1.0
1.5
2.0
2.5
3.0
3.5
4.0
4.5
5.0
0.0
0.5
1.0
1.5
2.0
2.5
3.0
Normalized Mean Stress, Po/q

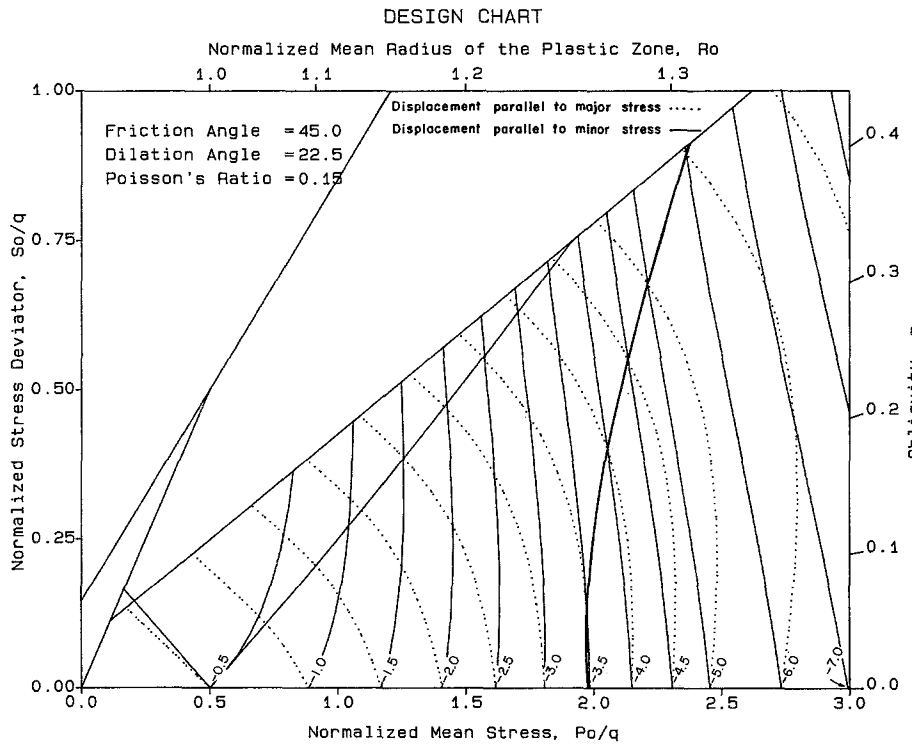
DESIGN CHART
Normalized Mean Radius of the Plastic Zone, Ro
1.0
1.1
1.2
1.3
Displacement parallel to major stress .....
Displacement parallel to minor stress ——
Friction Angle =45.0
Dilation Angle =22.5
Poisson's Ratio =0.15
Normalized Stress Deviator, So/q
1.00
0.75
0.50
0.25
0.00
Obliquity, m
0.4
0.3
0.2
0.1
0.0
0.5
1.0
1.5
2.0
2.5
3.0
3.5
4.0
4.5
5.0
6.0
7.0
0.0
0.5
1.0
1.5
2.0
2.5
3.0
Normalized Mean Stress, Po/q

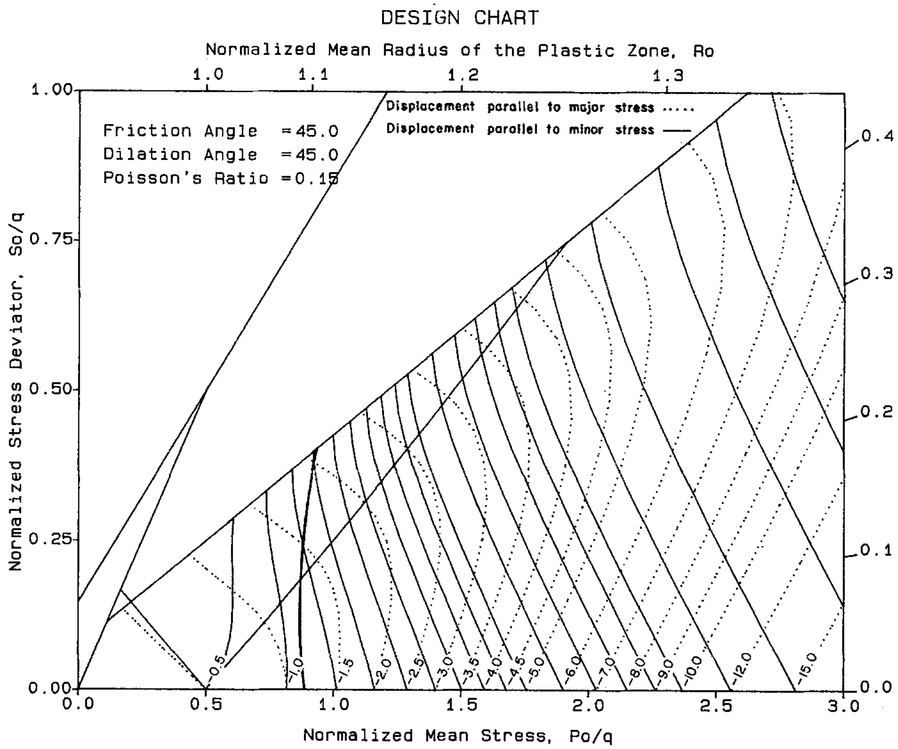

References

Brown, E. T., et al. (1983): Ground Response Curves for Rock Tunnels. J. Geotechnical Engineering, ASCE *109*, 15—39.

Detournay, E., Fairhurst, C. (1982): Generalization of the Ground Reaction Curve Concept. 23rd U.S. Symposium on Rock Mechanics, Berkeley, pp. 926—936.

Detournay, E. (1985): Solution Approximative de la Zone Plastique Autour d'une Galerie Souterraine Soumise à un Champ de Contrainte Non-Hydrostatique, C. R. Académie des Sciences, Paris, *301:12*, 857—860.

Detournay, E. (1986a): An Approximate Statical Solution of the Elastoplastic Interface for the Problem of Galin with a Cohesive-Frictional Material. Int. J. Solids Structures, *22*, 1435—1454.

Detournay, E. (1986b): Elastoplastic Model of a Deep Tunnel for a Rock with Variable Dilatation. Rock Mechanics and Rock Engineering, *19*, 99—108.

Detournay, E., Fairhurst, C. (1986): A Two-Dimensional Elastoplastic Analysis of a Long Cylindrical Cavity Under Non-Hydrostatic Loading. Int. J. Rock Mechanics and Mining Sciences, *24*, 197—211.

Galin, L. A. (1946): Plane Elastic-Plastic Problem: Plastic Regions Around Circular Holes in Plates and Beams. Prikladnaia Matematika i Mechanika, *10*, 365—386.

Hoek, E., Brown, E. T. (1980): Underground Excavations in Rock. London: The Institution of Mining and Metallurgy.

Hill, R. (1967): The Mathematical Theory of Plasticity. London: Oxford University Press.

Kachanov, L. M. (1971): Foundations of the Theory of Plasticity. Amsterdam: North-Holland Publishing Company.

Masseau, J. (1899): Mémoire sur l'Intégration Graphique des Equations aux Derivées Partielles. Ann. Ass. Ing. Ec. Gand. (Reprinted as Edition du Centenaire, Comité National du MECE, Brussels.)

Muskhelishvili, N. I. (1962): Some Basic Problems of the Mathematical Theory of Elasticity. Groningen: Noordhoff.

Newmark, N. M., et al. (1970): Ground Motion Technology Review. SAMSO, TR-70-114, Nathan M. Newmark Consulting Engineering Services.

Prager, W., Hodge, P. G. (1968): Theory of Perfectly Plastic Solids. New York: Dover.

Salencon, J. (1969): Contraction Quasi-Statique d'une Cavité à Symétrie Sphérique ou Cylindrique dans un Milieu Elastoplastique. Annales des Ponts et Chaussées, *4,* 231—236.